

Optimizing Continuous-Wave Pumped Entanglement-based QKD in Noisy Environment

Hashir Kuniyil^{1,*}, Saif Al-Kuwari^{1,†}, Asad Ali¹, Artur Czerwinski², and Syed M. Arslan¹

¹*Qatar Centre for Quantum Computing, College of Science and Engineering, Hamad Bin Khalifa University, Doha, Qatar*

²*Institute of Physics, Faculty of Physics, Astronomy and Informatics,*

Nicolaus Copernicus University in Torun, ul. Grudziadzka 5, 87-100 Torun, Poland

(Dated: February 25, 2025)

Quantum key distribution (QKD) has emerged as a promising solution to protect current cryptographic systems against the threat of quantum computers. As QKD transitions from laboratories to real-world applications, its implementation under various environmental conditions has become a pressing challenge. Major obstacles to practical QKD implementation are the loss of photons in the transmission media and the presence of extreme noise, which can severely limit long-range transmission. In this paper, we investigate the impact of extreme noise on QKD system parameters, including detector timing uncertainty (jitter), measurement timing shifts, variations in detector deadtime, and rate-dependent detector efficiency. Contrary to manufacturers' specifications, which assume these parameters to be constant, we demonstrate that these parameters exhibit significant variations in extreme noise conditions. We show that changes in these parameters play a key role in determining system performance in noisy environments. To address these non-idealities, we develop a robust model that can address and adapt to various detector characteristics. In particular, our model is independent of source parameters and can be implemented using data from the detection unit. Our results show that our model is well suited for characterizing and optimizing the performance of the QKD system under noisy conditions.

Keywords: Quantum key distribution, entanglement, coincidence measurement, avalanche photodetector, coincidence window optimization.

I. INTRODUCTION

Quantum key distribution (QKD) is a method for securely transferring keys between multiple parties using quantum mechanics. QKD uses the no-cloning theory to detect unauthorized access in a two-party cryptographic communication [1, 2] and have been developed in various forms [3–8], including quantum-entanglement-based QKD protocols[5, 7] and twin-field and decoy-state prepare-and-measure implementations [3, 4]. This system can further be extended to correct instrument-imposed loopholes with the assistance of device-independent QKD protocols [6, 9].

These QKD methods have proven successful in both laboratory and practical settings, and significant efforts have been focused on extending the distance of individual quantum links using fiber-based communications [10–12] and free space connections, including terrestrial links [13–15] and satellite communications [16, 17].

However, practical QKD faces major challenges, including higher noise levels and increased loss, which make the implementation of the protocol difficult. Unlike fiber-based connections, which are relatively immune to extreme noise, free-space links are more prone to intense noise interference [15, 18]. One way to reduce noise is spectral filtering, but its effectiveness is limited in extremely noisy environments [15]. Temporal filtering offers additional noise filtering, taking advantage of the temporal correlation of the source's photons to remove unwanted photons [13, 15, 19]. Nevertheless, temporal filtering becomes ineffective in scenarios where noise photons are predominantly higher where the detector cannot

function at this level of noise. Therefore, the aim is to maximize the performance within the functional level of noise of the detector.

In [20], the authors achieved high performance by optimizing the coincidence window considering detector jitter, photon loss, and source photon's pair rate. Their experimental study considered a QKD system operating in the telecommunication band and used superconducting nanowire single-photon detectors (SNSPDs). However, non-linear imperfections of the detectors, that can arise due to higher photon detection, have not been considered.

Similarly, the authors in [21] conducted experiments to investigate variations in detector parameters, including dead time, timing jitter, detection timing shift, and afterpulsing effects as a function of detection count rate. They studied these parameters by sending pulsed laser light with well-controlled photon time separation to an actively quenched avalanche photodetector operated in a Geiger mode. Their results showed that these parameters are not constant and demonstrated a method to correct for these variations. This method is useful for mitigating deterioration factors in noisy detection. However, in continuous-wave (CW) sources, photon timing is not well-controlled and is governed by photon statistics.

In this paper, we performed an experiment to investigate and determine changes in detector parameters during high-photon detection events in CW-pumped systems. From the insight gained from this study, we develop a model to describe the coincidence measurement of the system and its dependence on variations in the timing jitter, detector dead time, and detection timing shift.

To characterize and analyze the QKD system under high noise condition, we employed spontaneous parametric down-conversion (SPDC) [22, 23] process as a quantum source and an external broadband noise source features the noise photons. SPDC is a widely used quantum source for QKD realization,

* hkuniyil@hbku.edu.qa

† smalkuvari@hbku.edu.qa

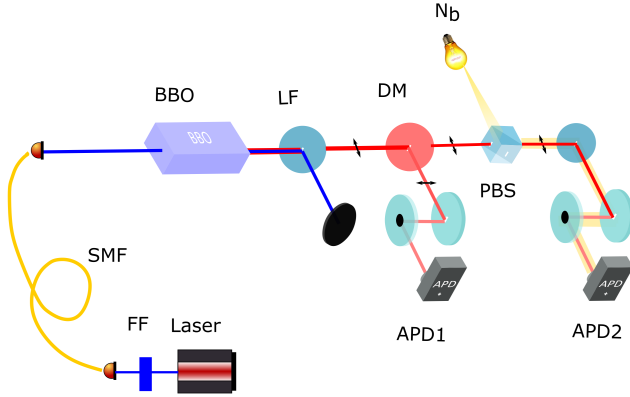


FIG. 1: Schematic of the experimental setup for coincidence profile characterization in noisy environments. FF - fluorescent filter, LF - long pass filter, SMF - single mode fiber, DM - dichroic mirror, N_b - noise source, PBS - polarizing beam splitter.

and the characteristics of broadband noise resemble noise expected in a practical system. Therefore, our method simulates a realistic scenario. Our findings from a single basis experimental study were extended to a two-basis theoretical model. This model enables the analysis of critical parameters of the QKD, including secure key rate (SKR), quantum bit error rate (QBER), and acceptable noise-photon levels within the coincidence window size of the system. Analyzing these parameters is crucial to improve system performance, particularly in extremely noisy environments.

The rest of this paper is organized as follows: In Section II, we discuss the effect of noise on coincidence measurements and present a simple experimental setup for this study. Part of this section also deals with the characterization of detector parameters, including timing jitter, afterpulsing, and detection timing shift. Section III presents a theoretical analysis of a two-basis entanglement QKD system, which leads to the optimization of the coincidence measurement window. Finally, Section IV provides concluding remarks about our study.

II. EXPERIMENTAL ANALYSIS

A. Experimental Setup

Fig. 1 shows the experimental setup we use to conduct detector characterization and coincidence measurement analysis. In this experiment, a spatially and spectrally filtered CW laser acts as a pump source with a central wavelength of 405 nm, and bandwidth of 160 MHz, which impinges on a type I configured 6 mm long beta-barium borate (BBO) crystal. As a result, two copolarized and nondegenerate signal and idler photons with wavelengths of 780 and 842 nm are generated, respectively. These two photons are later separated using a dichroic mirror (DM). Signal photons are directly detected by a passively quenched single-photon avalanche photodetector

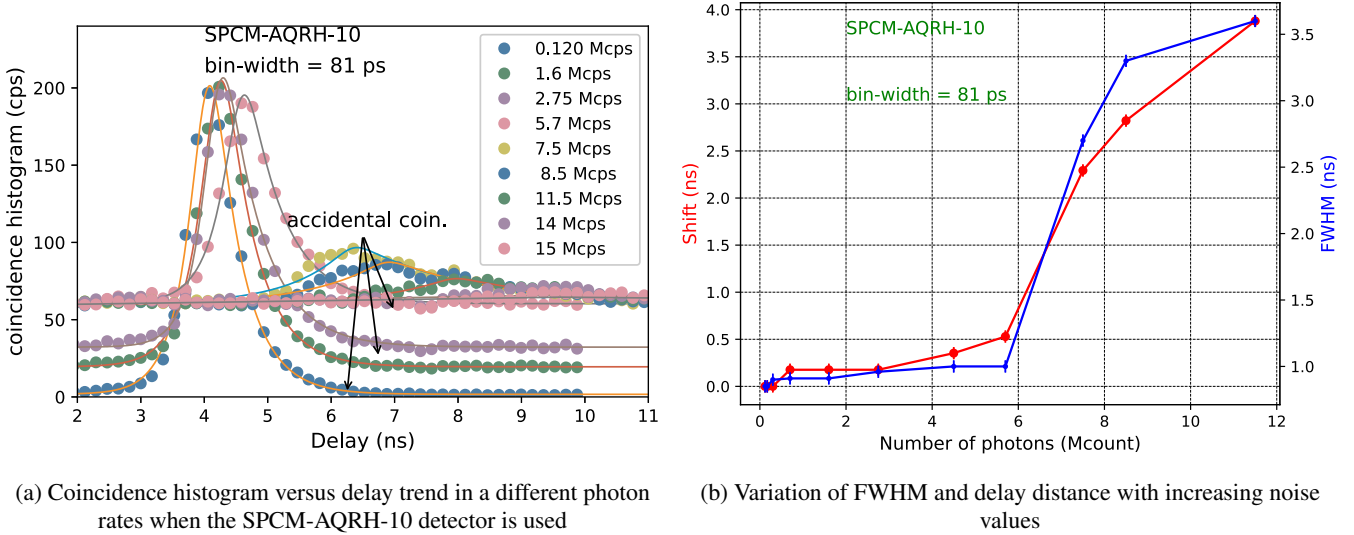
(APD1). The other photon, the idler, passes through a polarizing beam splitter (PBS), and then detected by an actively quenched APD operated in the Geiger mode (APD2). The noise source is directed towards APD2 by sending it from the perpendicular face of the PBS with respect to the idler photons. The noise source we used is a nonpolarized incandescent lamp that demonstrates thermal photon statistics.

In our experiment, only APD2 received noise (APD1 is shielded from noise). Therefore, the measured output from APD2 is a mixture of signal and noise. These two detectors are connected to a timestamp unit (not shown in Fig. 1) to record the time of arrival of individual photons received at both detectors. By analyzing the joint time of arrival of the photons at the detectors, we could obtain a temporal coincidence histogram as shown in Fig. 2a. In the experiment, idler photons travel 1.2 m extra optical path (equivalently, a 4.2 ns shift in the time axis); therefore, the coincidence histogram has an offset from zero point as evident from Fig. 2a. In the experiment, we used the passive detector made by S15 (with maximum count rate: 120 k cps, timing jitter 250 ns) as APD1, and the Excelitas detector (SPCM-AQRH-10) as APD2. Table I shows the important parameters of the Excelitas detector.

B. Coincidence Measurement in Noisy Settings

In a typical QKD protocol (e.g., BBM92 protocol [7]), Alice and Bob each require a minimum of two detectors to distinguish orthogonal quantum states. This requirement stems from the protocol's security mechanism, which relies on the quantum nature of a maximally entangled state and necessitates measurements in two bases. Implementing the protocol requires examining the coincidence counts of measurement events between Alice and Bob using two detector combinations. Therefore, single-basis experimental settings are not sufficient for a complete protocol implementation. However, to study the factors affecting SKR and QBER and their performance changes due to operation in a noisy environment, examining the two detection coincidence events should be sufficient. One key difference is that the photon coincidence rate obtained by a single basis system will be twice that of two basis measurements. Additionally, it is important to note that by considering only one detector at Alice and Bob locations, we are ignoring the polarization error from the basis setting. This is justifiable as this factor will contribute less than 1% of the total errors [24]. However, this leads to a multiplicative change in the overall error rate.

Fig. 2a shows a plot generated under various noise conditions (the actual noise values are indicated in the figure). In our analysis, the number of coincidences is determined by accumulating the number of coincidence events every second. By compiling the experimental coincidence values, we can obtain a full coincidence events' distribution that provides important information about the system. The width of the coincidence events is proportional to the timing jitter of the detector. The Excelitas detector has timing jitter of 0.35 ns according to the manufacturer, which we verify by measuring the full-width at



(a) Coincidence histogram versus delay trend in a different photon rates when the SPCM-AQRH-10 detector is used

(b) Variation of FWHM and delay distance with increasing noise values

FIG. 2: Effects of noise on the performance of single-photon detectors.

half-maximum (FWHM) of the coincidence distribution in a low noise condition. The S15 detector has slightly less timing jitter, namely 0.25 ns. We observed four distinct changes in the coincidence events as a function of increasing noise.

1. A proportional time shift in the coincidence events with an increase in noise
2. An increase of the FWHM of the coincidence distribution as the noise increases
3. An increase in the floor level of the coincidence events (minimum value of the observed coincidence events) due to noise events
4. The height of the coincidence histogram started reducing beyond detection threshold of 4.5 Mcps

Not all photon pairs generated in the SPDC process are detected. Due to photon loss during the transmission, the heralding efficiency of the system is degraded and it can be approximated using

$$S = B\eta, \quad (1)$$

where B is the number of pairs generated, η is the detection efficiency. η is inclusive of all loss parameters such as transmission loss, detector efficiency, coupling efficiency. With this, the probability of simultaneously arriving photons in both detectors can be estimated with

$$C = B\eta_A\eta_B. \quad (2)$$

Where η_A and η_B are the detection efficiencies of channel A and channel B, respectively. The detection events reported by the detectors also have noise photons, such as the dark count of the APDs and stray noise entered in the detectors. which can be modeled by modifying Eq. (1) as

$$S_A = B\eta_A\eta_B + N_A + DC_A \quad (3)$$

$$S_B = B\eta_A\eta_B + N_B + DC_B, \quad (4)$$

where N_A and N_B are the count of noise entered in detector A and detector B, DC_A and DC_B are the dark count rates of detector A and detector B, respectively. In the measurement, there is a random probability that two uncorrelated photon events fall within the same time window, even though they are not from the SPDC process. This is known as accidental coincidence events. These events are the primary source of noise in coincidence-based measurement. Therefore, the rate of accidental coincidence increases with the noise photons. With this, the accidental coincidence is calculated by multiplying single events from two detectors with the chosen coincidence time window which can be written as

$$N_{AC} = S_A S_B \tau_{cw}, \quad (5)$$

where τ_{cw} is the chosen coincidence time window. In Fig. 2a, the accidental coincidence can be estimated by measuring the minimum value read on the coincidence axis. As the dark count of a detector is constant and is known from the manufacturer, the environment-imparted change in the detection events is the only varying parameter. As we do not have another reference for total events and the measured value of detection counts has all parameters, we could estimate accidental coincidences by knowing the coincidence time widow we chose using Eq. (5). With this, we have found that Eq. (5) is consistent with the observed values of S_A and S_B with the chosen τ_{cw} . Typically, real coincidence events are theoretically approximated using a normal distribution of the form [25, 26]

$$j(\tau) = \frac{1}{\sigma\sqrt{2\pi}} \exp\left(-\frac{\tau^2}{2\sigma^2}\right), \quad (6)$$

where σ is the detector jitter and τ is the measurement time. This method can be applied in numerical simulations to investigate quantum state tomography of entangled qubits with measurements affected by time uncertainty [27]. However, this approximation fails when systems operate in extreme noise regimes. Also, this approximation does not allow one to study individual detector characteristics from the coincidence histogram. In our experiment, where only one detector receives noise-induced clicks, the probabilistic distribution of the coincidence events does not show a clean Gaussian profile in the high noise regime, rendering a normal distribution that does not fit our collected data. Neumann *et al.* [20] investigated coincidence events using the normal distribution function for various coincidence values, accounting for variations in the Full Width at Half Maximum (FWHM) and shifts caused by dispersion in optical fibers. Using the detector function of the form of Eq. (6), they characterized the changes in the detector parameters using linear functions. In contrast, our observations reveal a polynomial growth in FWHM (see Fig 2b) and a shift in the coincidence time. This discrepancy arises because previous work assumed equal photon pair detection rates across all detectors in a low-noise scenario (in our case, if noise photons entered <4.5 Mcps, the widening of FWHM will appear almost linear). Consequently, in their study, FWHM changes and coincidence peak shifts appeared linear.

Our results show noise photon can be responsible for shift in the detection timing, particularly its evident when detection rates are imbalanced between detectors. To address this, we should be able to cater to the changes in individual detectors reflect in the theoretical fit. By incorporating noise-induced variation parameter with exponential distribution coincidence histogram, we could detect changes in the individual detectors as follows

$$G = N_{AC} + B\eta_A\eta_B(1 - t_{dA}S_A\eta_A)A_i + B\eta_A\eta_B(1 - t_{dB}S_B\eta_B)A_j \quad (7)$$

$$\begin{aligned} A_i &= e^{W_i\tau} && \text{for } \tau > C \\ A_j &= e^{-W_j\tau} && \text{for } \tau < C, \end{aligned} \quad (8)$$

where $W_{s(i)}$ is a coefficient used to accommodate the change in the width of coincidence events, t_d is the dead time of the detector and C is the centroid value of the coincidence histogram. $1/W$ will provide the FWHM in the time domain. By convoluting detector function in Eq. (6) with A_i and A_j , we can obtain a complete coincidence histogram function of the form:

$$\begin{aligned} C(\tau, W_s, W_i, t_D) &= S_A S_B \tau_{cw} + B\eta_A\eta_B(1 - t_{dA}S_A\eta_A) \\ &\quad e^{W_s(W_s\sigma_s^2/2 + \tau - t_D)} \text{erfc} \left[\frac{W_s\sigma_s^2 + \tau - t_D}{\sqrt{2}\sigma_s} \right] \\ &\quad + B\eta_A\eta_B(1 - t_{dB}S_B)e^{W_i(W_i\sigma_i^2/2 - \tau + t_D)} \text{erfc} \left[\frac{W_i\sigma_i^2 - \tau + t_D}{\sqrt{2}\sigma_i} \right], \end{aligned} \quad (9)$$

where σ_s and σ_i are the timing uncertainty (jitter) of the detectors used at signal and idler arms, respectively, t_D is the shift

of centroid point of coincidence histogram from the origin, and “erfc” represents the complimentary error function. Detector timing jitter is predominantly responsible for the width of the coincidence events. The timing uncertainty of the detectors (jitter) is responsible for the width of the coincidence histogram plots. If the temporal coherence of the collected photons is significantly greater than the jitter of the detection system, the measured spectral profile will reflect the true spectral characteristics of the photons more closely [28, 29]. The coherence time of our photon pairs is about 21.5 fs (corresponding to the spectral bandwidth of 30 nm), which is negligible and overshadowed by the timing jitter of the detectors. Therefore, timing uncertainty due to this factor could be omitted. Additionally, the temporal resolution of the timestamp unit also contributes to the width of coincidence events if it is greater than the timing jitter. Since the temporal resolution of our timestamp unit is 81 ps, we can omit this factor as well. When the noise is low, we can approximate $W_{s(i)} = 1/\sigma_{s(i)}$. As noise increases, we adjusted the value of $W_{s(i)}$ to fit with the experimental data. Theoretical fit for the collected experimental data is shown in Fig. 2a. The change in the FWHM in different noise settings is shown in Fig. 2b. We observe that $W_{s(i)}$ is proportional to the FWHM of the coincidence histogram. The experimentally obtained shift of the start-stop histogram was directly incorporated into Eq. (9) during data fitting. One parameter that largely depends on the shape of the coincidence histogram is the variation in the dead time of the detectors due to high photon detection events. We have investigated the change in dead time with increased event rates in the detector. We used experimentally obtained t_d values (discussed in Section II C) in our model.

Parameter	SPCM-AQRH-10
deadtime	22 ns
timing jitter	350 ps
maximum count	17.00 MHz
efficiency@ 780 nm	59 %
active area	180 um
Dark count	25 cps

TABLE I: Certified SPCM-AQRH-10 detector’s parameters.

C. Characterization of Detector Parameters

The SPCM-AQRH-10 detector is a commonly used single-photon detection module in QKD. This is an actively quenched Geiger mode detector, and the manufacturer-provided parameters of this detector are summarized in Table I. To study the count rate-dependent detector parameters, from the experimental setup described in Fig. 1, we only considered the APD2 output and investigated detector parameters such as detector dead time and twilight events. For this, the singles values recorded from APD2 were subtracted from their neighboring photon time values, that is, $\Delta t = t_{n+1} - t_n$ where t is the time of arrival of photons and n is the index value. The number of measured time separations (Δ) is plotted as a histogram in Fig. 3. This figure gives interesting results about

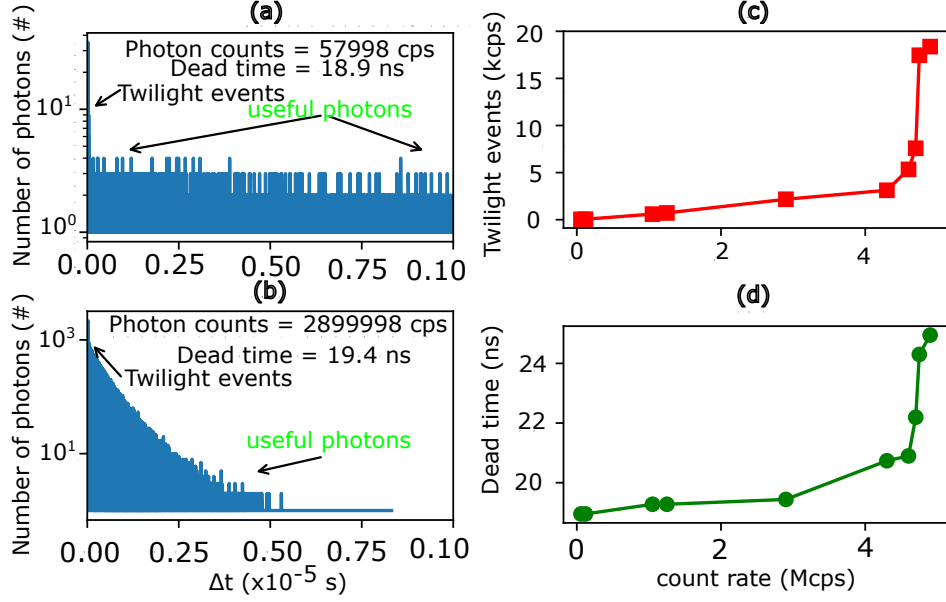


FIG. 3: (a) and (b) SPCM-AQRH-10 detector characteristic feature changes in the events of low and high count rates (values of dead time and photon counts are given in the inset). (c) showing the values of twilight events in various count rates and (d) shows the trend in the dead time in different count rates

many detector parameters, including dead-time and twilight events. The dead time in single-photon avalanche photo detectors [21] is often described as a temporal window in which photons cannot be detected, which means that the dead time can be estimated by knowing the separation from 0 to the offset value of Δt time in Fig. 3.

We observed that the dead time is not constant but increases with the count rate. This observation contradicts the common assumption that detector dead time is constant. An increasing dead time with higher count rates suggests that the detector recovery dynamics is more complex. Under high illumination, the internal circuitry may take more time to fully reset, possibly due to saturation effects or an increased thermal load.

The varying detector dead time can influence the temporal shift of the coincidence histogram discussed in the Section II B. That is, the dead time can be defined as an interval that spans the quenching and resetting time. In this interval, there is a time zone called the twilight zone, where the detector is semi-sensitive, and photons may be sensed but will not be reflected until the detector completes resetting. This means that the photons in the twilight zone must wait for a period of time to be registered. This waiting period is responsible for a delay in the cross-correlation function. The dead time and twilight events are shown in Fig. 3 in two cases of noise values. As illustrated, the twilight events occur close to the dead time of the detectors because if two photons arrive at the detectors closer to the dead time, the lagging one will have to wait for the dead time to end or will not be registered at all. If a large number of photons are sent to the detectors, this scenario will happen more frequently, and so the twilight event becomes

significantly high. The measured values of the twilight events and the dead time for various noise levels are shown in Fig. 3 in panels (c) and (d). The change in twilight events and dead time increased sharply after the noise level passed 4.5 Mcps. This is in proportion to an observed shift in the coincidence histogram where shift and FWHM also drastically changed after reaching this onset value.

III. THEORETICAL ANALYSIS

Given the trend of coincidence events in the presence of extreme noise, one should investigate its influence on the SKR and QBER. Typically, a coincidence window (a chosen measurement time window to observe coincidence events) is optimized to achieve a maximum SKR with a manageable QBER. Due to the Gaussian shape of coincidence events, optimal coincidence window selection is crucial for improved QKD performance. Additionally, the change in the shape of the coincidence histogram due to extreme noise should also be considered when choosing the coincidence window.

In this section, we theoretically investigate the factors to consider when determining the coincidence window in a QKD system. We first investigate influencing factors in a single-basis measurement setting and then study effects on a complete two-basis QKD system.

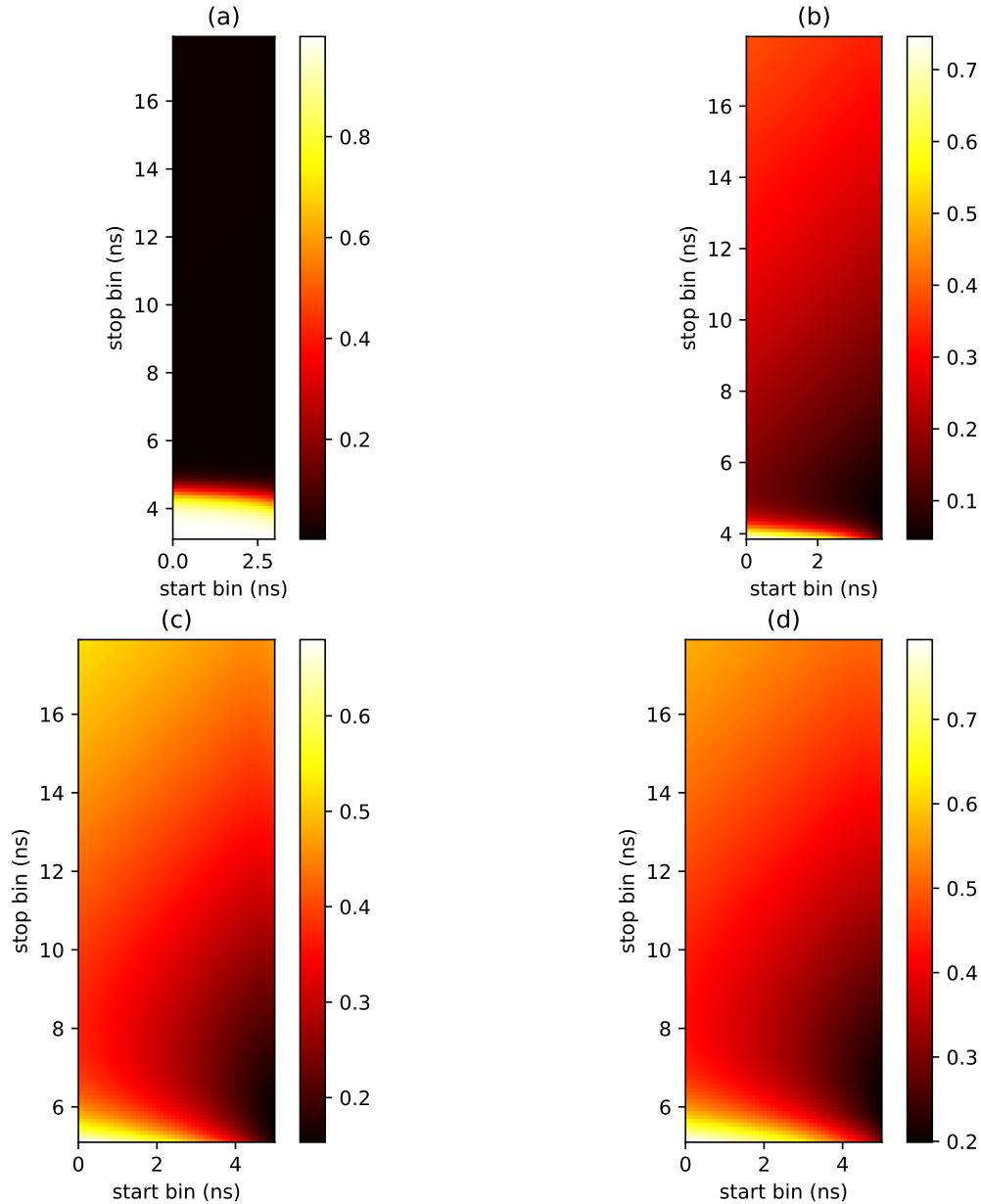


FIG. 4: Accidental coincidence over actual coincidences in a choice of various start-bin and stop-bin values in the noise events
 (a) 100 kcps (b) 4 million cps (c) 13 million cps and (d) 17 million cps.

A. Coincidence Measurement in a Single Basis System

Eq. (9) provides a complete measurement result, including the noise effect on the coincidence profile. Therefore, the total coincidence values within the chosen coincidence window can be estimated by carrying out the integration

$$E = \int_a^b C(\tau, W_s, W_i, t_D) d\tau. \quad (10)$$

Where E is the total number of coincidence events with start-bin a and stop-bin b . When we determine the start-bin and stop-bin values and compute the total coincidence events, E ,

using Eq. (10), the result will contain all coincidence events including coincidence events from generated photon pairs and accidental coincidence events. Also, it will have a detector efficiency factor, as our model has accounted for it. When the detectors operating in a low noise regime, the share of accidental coincidence in the computed “C” value is low. In this case, it is desirable to select a wide coincidence window. However, in extreme noise events, the share of accidental coincidence is higher, and the target in this case would be to minimize the accidental coincidences so that QBER can be lowered. The QBER and accidental coincidence are directly proportional and therefore, in a single basis system, minimiz-

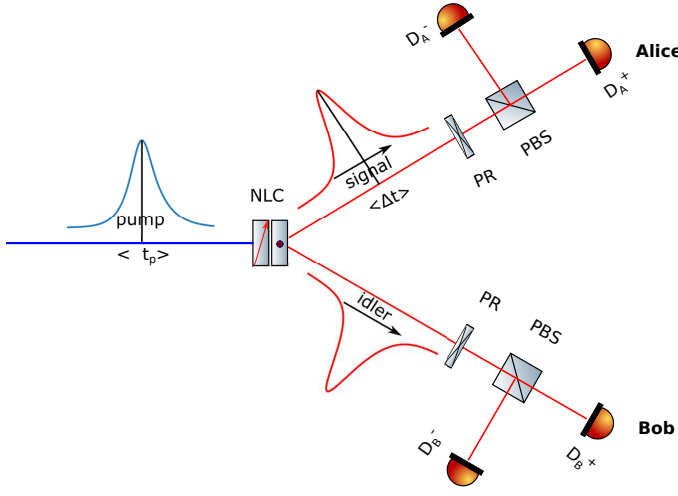


FIG. 5: Typical experimental setup used to implement BBM92 QKD protocol. NLC - nonlinear crystal, PR - polarization rotator, PBS - polarizing beam splitter.

ing the ratio of accidental coincidence with total coincidence would be one target parameter that could approximate QBER measurement, i.e.

$$E_r = \frac{N_{AC}}{E}. \quad (11)$$

Fig. 4 shows the values of E_r for different start and stop bin values, where the coincidence window size is defined as the difference between the stop and start bins (stop bin - start bin). When noise is low, E_r reaches desirable low levels, with an observed value of $E_r = 0.1\%$ in this case. As noise increases, the values of E_r increase accordingly to 7. 59%, 15. 32%, and 19. 9% for Figs. 4 (b), (c), and (d), respectively.

Since the width of the coincidence histogram increases with noise, different start and stop bin values must be considered to achieve a lower E_r . We selected the following start and stop bin values (in ns): 3 and 4.6, 3.75 and 5.05, 5 and 6.3, 5 and 6.3, respectively. Notably, the start bin value must be adjusted to correct for the shift in the coincidence histogram's peak position.

B. QKD Performance Under Noisy Conditions

To analyze the changes in the complete QKD system due to noise, measurements in at least two bases are necessary. This requires Alice and Bob to each have two detectors, with the capability to randomly select the basis from a two conjugate basis set. To satisfy this condition, the quantum source in entanglement-based QKD must generate Bell states, which can be defined as:

$$|\psi\rangle = \alpha |H_A H_B\rangle + \beta |V_A V_B\rangle, \quad (12)$$

where quantum states $|H\rangle$ and $|V\rangle$ represent horizontal and vertical polarization, respectively, while the subscripts A and

B denote Alice and Bob photons, respectively. The parameters α and β represent amplitudes with probabilities given by $|\alpha|^2$ and $|\beta|^2$, respectively, such that $|\alpha|^2 + |\beta|^2 = 1$. In a balanced system, $\alpha = \beta = 1/\sqrt{2}$. Thus, the probabilities for $|HH\rangle$ and $|VV\rangle$ are equal. In the implementation of a typical QKD protocol, bases are randomly set into two states (in BBM92 bases 45° and 0° are randomly set). Statistically, half of the total photon pairs generated will undergo measurement in the 45° basis, while the remaining half will be measured in the 0° basis. Therefore, there must be at least two coincidence measurements, one between detector D_A^- and D_B^- and the other between D_A^+ and D_B^+ (see Fig. 5). To understand the total coincidences in this case, we can modify Eq. (10) and obtain

$$C = \int_{A^+}^{B^+} C^+(\tau, t_\Delta^+, t_D^+) + \int_{A^-}^{B^-} C^-(\tau, t_\Delta^-, t_D^-) d\tau, \quad (13)$$

where '+' and '-' indicate the positions of the detectors in the experiment as depicted in Fig. 5. Eq. (13) will provide complete coincidence values generated with the flexibility to select the coincidence window. Notice that the B value in Eq. (9) will turn to $B/2$ as total generated photon pairs must be equally shared between detectors. With this, the QBER (Q) of the system can be defined as

$$Q = 1/2(A^+ + A^-)/C, \quad (14)$$

where A^+ is the accidental coincidence between '+' detectors, and A^- is the accidental coincidence between '-' detectors. We could evaluate A^+ and A^- by using the following

$$A^{+(-)} = S_A^{+(-)}(1 - t_{dA^{+(-)}})S_B^{+(-)}(1 - t_{dB^{+(-)}})\tau_{cw} \quad (15)$$

When implementing the protocol, Alice and Bob randomly switch their measurement basis between 0° and 45° . Next, they publicly reveal their basis choice. Due to random selection, they have a 50% probability of choosing the correct basis. Only compatible basis choices are considered for protocol implementation, hence, 50% of the coincidence measurements are discarded. Therefore, the total achievable secure key rate (R) in this procedure could be given by [30]

$$R = \frac{1}{2}C[1 - f(Q_{bit})H_2(Q_{bit}) - H_2(Q_{phi})], \quad (16)$$

where $H_2(x)$ is the binary entropy function, defined by

$$H_2(x) = -x \log_2 x - (1 - x) \log_2(1 - x), \quad (17)$$

where Q_{bit} is the error in bit streams, Q_{phi} is the phase error between $|H\rangle$ and $|V\rangle$ polarization states, and $f(Q_{bit})$ accounts for the additional bits sacrificed during the reconciliation process to ensure Alice and Bob share an identical key sequence. Reconciliation is a crucial step in QKD, where classical error correction protocols are applied to correct discrepancies in the sifted key while minimizing information leakage to a potential eavesdropper. As a realistic value of $f(Q_{bit}) \leq 1.1$ [31], we considered the maximum limit while executing the

model. Due to the symmetry of the basis choice, we can consider $Q_{phi} = Q_{bit} = Q$. Incorporating these, finally we turn Eq. (16) into

$$R = \frac{1}{2}C[1 - 2.1H_2(Q)]. \quad (18)$$

Using Eq. (18) and (14), we examine SKR and QBER in noisy scenarios. With a pair rate (B) of 500K cps distributed equally at the Alice and Bob sites, Fig. 6 illustrates the trend of SKR and QBER in various noise levels for different start-bin and stop-bin choices. In this demonstration, we considered equal noise distributed to all detectors. The result shows that a QBER threshold of $Q = 0.102$ (indicated by the dark dotted line in Fig. 6) is established, above which no secure key can be generated. At this threshold, the secure key rate becomes zero ($R = 0$). Therefore, achieving $Q < 0.102$ is a target for the implementation of QKD. To reach this threshold, different start and stop bin choices tolerate different levels of noise. For example, when the start bin = 3 ns and the stop bin = 6 ns, the system tolerates 26 million noise counts before reaching $R = 0$. However, it accepts 17 million noise counts when the start of the bin = 1 ns and the stop bin = 8 nm, despite the larger total coincidence window. When the start bin is set near the centroid of the coincidence window (the start bin = 4.5 ns) and the stop bin = 7.5 ns, the system shows reduced resistance to noise, tolerating only 13.5 million noise counts.

C. Optimization of Coincidence Window

To improve the secure key rate (R) value even in higher noise counts, we narrow the coincidence window by adjusting the start and stop bin (because of the Gaussian-like profile of the coincidence histogram). Taking this into account, we selected the start-bin (a) = 4 ns and the stop-bin (b) = 5 ns. As expected, the noise immunity for this choice showed better performance, requiring 32 Mcps to reach $R = 0$. However, the problem with this choice of coincidence window is the reduced secure key rate when the noise is lower. To optimize the coincidence window, we apply the Broyden-Fletcher-Goldfarb-Shanno (BFGS) algorithm with the objective condition:

$$\min_{a,b \in \mathbb{R}^n} f(x). \quad (19)$$

The objective function in our case is $f(x) = -R(a, b, N_1, N_2, N_3, N_4, B)$. Our aim is to maximize R with fixed noise values, and the photon pair rate (B). The negative value of R indicates the maximization in BFGS, where a and b are the variables. Therefore, in the BFGS formulation, we take $x = [a, b]$ and $\nabla f(x) = [-\partial R / \partial a, -\partial R / \partial b]$. With the initialization value x_0 and the initial Hessian function approximation $H_0 = I$, we calculate the gradient in each iteration k as $g_k = \nabla f(x_k)$ and the search direction $d_k = -H_k g_k$. The updates of the values of x in each iteration can be found using $x_{k+1} = x_k + \alpha_k d_k$, where α_k is the step size. We compute the differences $s_k = x_{k+1} - x_k$ and $y_k = \nabla f(x_{k+1}) - \nabla f(x_k)$ and

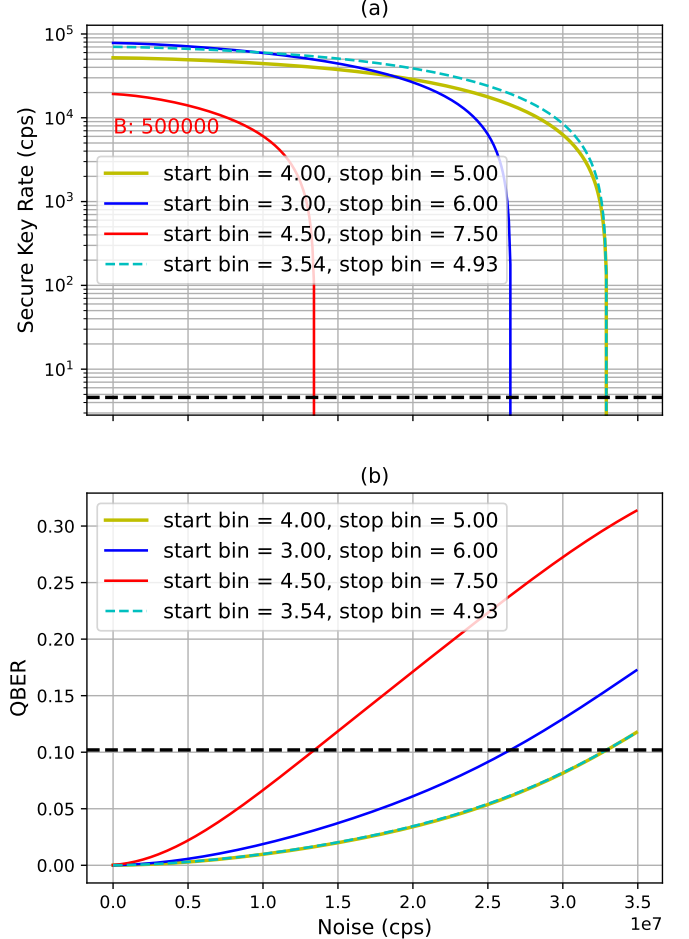


FIG. 6: Evaluated QKD parameters of secure key rate and QBER in noisy settings for a set of start and stop bin values. Different start and stop bin choices set the threshold of noise (dark dotted line) for SKR (a) and QBER. The dotted cyan line shows an optimized choice of coincidence window.

achieve the updated Hessian approximation as:

$$H_{k+1} = (I - \rho_k s_k y_k^T) H_k (I - \rho_k y_k s_k^T) + \rho_k s_k s_k^T, \quad (20)$$

where $\rho_k = 1/(y_k^T s_k)$. This process continues until $\|\nabla f(x_k)\|$ reaches a value less than the error tolerance. With the given values of N_1, N_2, N_3, N_4 and B , the BFGS algorithm can obtain a maximum value of R . Our requirement of achieving the best possible R value when the system is operating in a noisy environment can be satisfied. By assigning equal noise values to our model (with given total noise level $N = N_1 + N_2 + N_3 + N_4 = 22$ Mcps) and setting $B = 500$ Kcps, we found that with $a = 3.54$ ns and $b = 4.93$ ns, the system will give the best performance for the QKD system. With this choice of coincidence window, the system can be used to obtain 33,162 secure keys, reaching $R = 0$ when $N = 32$ Mcps. Following this theoretical model, one could examine QKD in a variety of experimental settings, including cases of QKD execution under high pair rate and low noise, high pair rate and high noise, and low pair rate and high noise. Additionally,

our model is suitable for the characterization of QKD systems in imbalanced detections where one detector receives many more photons than the others. This is especially the case in the entanglement-based QKD implementation where the source is on Alice's side [15].

The case presented in this work considered the pair rate of 500 Kcps. With previous techniques [24], it is possible to achieve pair rates as high as 10 Mcps and could also maximize the pair rate by following special techniques using bulk crystals [32]. The optimum values of start and stop bins will be different for different pair rates. This demonstrates the importance of characterizing the system parameters before employing them in practical use.

IV. CONCLUSION

In this paper, we propose an optimization method that allows efficient execution of entanglement-based QKD protocols in a noisy environment. We begin by considering a single-basis experimental setup to understand the factors affecting key QKD parameters in a CW-driven system. Although a single-basis system is insufficient for executing a complete QKD protocol, it simplifies the learning of individual factors that affect the system. We specifically investigate the factors influencing the nonideal behavior of detectors in continuous-wave (CW) driven QKD, identifying elements affecting practical models. We also presented a test to characterize detector functional changes owing to high photon rates. An experimental test to understand detector functional changes in a pulsed laser-driven QKD has previously been shown [21], where changes in detector parameters such as dead time, variation in jitter, and twilight effect were investigated. Contrary to CW-QKD, pulsed lasers offer full control of the pulse time interval, including the adjustment of undesirable detection timing shifts. This would not be straightforward in a CW-driven QKD, particularly because this effect can adversely affect performance if detection rates are imbalanced. In this scenario, our model will be helpful for analysis and optimization.

Incorporating these findings from the single-basis system, we

develop a theoretical model applicable to a two-basis system. Given the novelty of this effect, developing an optimization model is crucial. We introduce a simple and efficient model useful for identifying and addressing detector non-idealities that degrade QBER and SKR. The advantage of our developed model is its wide applicability across various QKD protocols, as it is based on the coincidence measurement used in many, if not all, discrete variable entanglement-based QKD systems. Furthermore, our demonstrated noise-induced shift in detection timing events possibly threatens the overall security of QKD, as it is well known that shifts in coincidence detection event times can be exploited by eavesdroppers for the hacking of secret data [33]. More studies are needed to understand the extent to which this shift influences the security of the system. One possible solution to mitigate the rate-induced timing shift is to characterize detector efficiency versus input photon rate analysis, as shown in [34], and then discard all communication events when the photon rate exceeds the onset value of efficiency degradation. From our analysis, efficiency degradation and coincidence histogram shift dominated after 4.5 Mcps (although the rated maximum count rate of the detector used is much higher, 17 Mcps).

This study enables researchers to implement efficient strategies prior to system deployment. Furthermore, our findings will be valuable for research in quantum detection technologies. Finally, our analysis of the detector's jitter and its impact on photon detections in the time domain is essential for the development and assessment of time-bin-encoded QKD protocols [35].

V. ACKNOWLEDGMENT

The experiment was carried out by Hashir Kuniyil while working at Ozyegin University under a project funded by the Turkish Scientific and Technological Research Council (TÜB-TAK) with Project No. 118E991. The idea development and all subsequent processing, including theoretical analysis and manuscript writing, were performed by the listed authors, including Hashir Kuniyil, at their respective institutions.

[1] C. H. Bennett and G. Brassard, Quantum cryptography: Public key distribution and coin tossing, in *Proc. IEEE International Conference on Computers, Systems and Signal Processing* (1984) pp. 175–179.

[2] C. H. Bennett and G. Brassard, Quantum cryptography: Public key distribution and coin tossing, *Theoretical Computer Science* **560**, 7 (2014).

[3] W.-Y. Hwang, Quantum key distribution with high loss: toward global secure communication, *Physical Review Letters* **91**, 057901 (2003).

[4] H.-K. Lo, X. Ma, and K. Chen, Decoy state quantum key distribution, *Physical Review Letters* **94**, 230504 (2005).

[5] A. K. Ekert, Quantum cryptography and bell's theorem, in *Quantum Measurements in Optics* (Springer, 1992) pp. 413–418.

[6] H.-K. Lo, M. Curty, and B. Qi, Measurement-device-independent quantum key distribution, *Physical Review Letters* **108**, 130503 (2012).

[7] C. H. Bennett, G. Brassard, and N. D. Mermin, Quantum cryptography without bell's theorem, *Physical Review Letters* **68**, 557 (1992).

[8] Z.-W. Yu, X.-L. Hu, C. Jiang, H. Xu, and X.-B. Wang, Sending-or-not-sending twin-field quantum key distribution in practice, *Scientific Reports* **9**, 1 (2019).

[9] D. Nadlinger, P. Drmota, B. Nichol, G. Araneda, D. Main, R. Srinivas, D. Lucas, C. Ballance, K. Ivanov, E.-Z. Tan, *et al.*, Experimental quantum key distribution certified by bell's theorem, *Nature* **607**, 682 (2022).

[10] Z.-D. Li, R. Zhang, X.-F. Yin, L.-Z. Liu, Y. Hu, Y.-Q. Fang, Y.-Y. Fei, X. Jiang, J. Zhang, L. Li, *et al.*, Experimental quantum repeater without quantum memory, *Nature Photonics* **13**, 644

(2019).

[11] F. Xu, X. Ma, Q. Zhang, H.-K. Lo, and J.-W. Pan, Secure quantum key distribution with realistic devices, *Reviews of Modern Physics* **92**, 025002 (2020).

[12] S. P. Neumann, A. Buchner, L. Bulla, M. Bohmann, and R. Ursin, Continuous entanglement distribution over a transnational 248 km fiber link, *Nature Communications* **13**, 6134 (2022).

[13] M. P. Peloso, I. Gerhardt, C. Ho, A. Lamas-Linares, and C. Kurtsiefer, Daylight operation of a free space, entanglement-based quantum key distribution system, *New Journal of Physics* **11**, 045007 (2009).

[14] C.-Z. Peng, T. Yang, X.-H. Bao, J. Zhang, X.-M. Jin, F.-Y. Feng, B. Yang, J. Yang, J. Yin, Q. Zhang, *et al.*, Experimental free-space distribution of entangled photon pairs over 13 km: Towards satellite-based global quantum communication, *Physical Review Letters* **94**, 150501 (2005).

[15] A. Kržič, S. Sharma, C. Spiess, U. Chandrashekara, S. Töpfer, G. Sauer, L. J. González-Martín del Campo, T. Kopf, S. Petscharnig, T. Grafenauer, *et al.*, Towards metropolitan free-space quantum networks, *npj Quantum Information* **9**, 95 (2023).

[16] C. C.-W. Lim, F. Xu, J.-W. Pan, and A. Ekert, Security analysis of quantum key distribution with small block length and its application to quantum space communications, *Physical Review Letters* **126**, 100501 (2021).

[17] S. Khatri, A. J. Brady, R. A. Desporte, M. P. Bart, and J. P. Dowling, Spooky action at a global distance: analysis of space-based entanglement distribution for the quantum internet, *npj Quantum Information* **7**, 4 (2021).

[18] S. Mishra, A. Biswas, S. Patil, P. Chandravanshi, V. Mongia, T. Sharma, A. Rani, S. Prabhakar, S. Ramachandran, and R. P. Singh, Bbm92 quantum key distribution over a free space dusty channel of 200 meters, *Journal of Optics* **24**, 074002 (2022).

[19] T. Kupko, M. von Helversen, L. Rickert, J.-H. Schulze, A. Strittmatter, M. Gschrey, S. Rodt, S. Reitzenstein, and T. Heindel, Tools for the performance optimization of single-photon quantum key distribution, *npj Quantum Information* **6**, 29 (2020).

[20] S. P. Neumann, T. Scheidl, M. Selimovic, M. Pivoluska, B. Liu, M. Bohmann, and R. Ursin, Model for optimizing quantum key distribution with continuous-wave pumped entangled-photon sources, *Physical Review A* **104**, 022406 (2021).

[21] M. Stipčević, B. G. Christensen, P. G. Kwiat, and D. J. Gauthier, Advanced active quenching circuit for ultra-fast quantum cryptography, *Optics Express* **25**, 21861 (2017).

[22] P. G. Kwiat, K. Mattle, H. Weinfurter, A. Zeilinger, A. V. Sergienko, and Y. Shih, New high-intensity source of polarization-entangled photon pairs, *Physical Review Letters* **75**, 4337 (1995).

[23] S. Karan, S. Aarav, H. Bharadhwaj, L. Taneja, A. De, G. Kulkarni, N. Meher, and A. K. Jha, Phase matching in β -barium borate crystals for spontaneous parametric down-conversion, *Journal of Optics* **22**, 083501 (2020).

[24] A. Anwar, C. Perumangatt, F. Steinlechner, T. Jennewein, and A. Ling, Entangled photon-pair sources based on three-wave mixing in bulk crystals, *Review of Scientific Instruments* **92** (2021).

[25] K. Sedziak-Kacprowicz, A. Czerwinski, and P. Kolenderski, Tomography of time-bin quantum states using time-resolved detection, *Physical Review A* **102**, 052420 (2020).

[26] A. Czerwinski, K. Sedziak-Kacprowicz, and P. Kolenderski, Phase estimation of time-bin qudits by time-resolved single-photon counting, *Physical Review A* **103**, 042402 (2021).

[27] A. Czerwinski, Quantum tomography of entangled qubits by time-resolved single-photon counting with time-continuous measurements, *Quantum Information Processing* **21**, 332 (2022).

[28] C. Clausen, F. Bussières, A. Tiranov, H. Herrmann, C. Silberhorn, W. Sohler, M. Afzelius, and N. Gisin, A source of polarization-entangled photon pairs interfacing quantum memories with telecom photons, *New Journal of Physics* **16**, 093058 (2014).

[29] B. Srivathsan, G. K. Gulati, B. Chng, G. Maslennikov, D. Matsukevich, and C. Kurtsiefer, Narrow band source of transform-limited photon pairs via four-wave mixing<? format?> in a cold atomic ensemble, *Physical Review Letters* **111**, 123602 (2013).

[30] X. Ma, C.-H. F. Fung, and H.-K. Lo, Quantum key distribution with entangled photon sources, *Physical Review A* **76**, 012307 (2007).

[31] D. Elkouss, J. Martinez-Mateo, and V. Martin, Information reconciliation for quantum key distribution, *arXiv preprint arXiv:1007.1616* (2010).

[32] H. Kuniyil and K. Durak, Efficient coupling of down-converted photon pairs into single mode fiber, *Optics Communications* **493**, 127038 (2021).

[33] A. Lamas-Linares and C. Kurtsiefer, Breaking a quantum key distribution system through a timing side channel, *Optics Express* **15**, 9388 (2007).

[34] H. Kuniyil, H. Ozel, H. Yilmaz, and K. Durak, Noise-tolerant object detection and ranging using quantum correlations, *Journal of Optics* **24**, 105201 (2022).

[35] J. Jin, J.-P. Bourgoin, R. Tannous, S. Agne, C. J. Pugh, K. B. Kuntz, B. L. Higgins, and T. Jennewein, Genuine time-bin-encoded quantum key distribution over a turbulent depolarizing free-space channel, *Optics Express* **27**, 37214 (2019).